M&C 2017 - International Conference on Mathematics & Computational Methods Applied to Nuclear Science & Engineering, Jeju, Korea, April 16-20, 2017, on USB (2017)

Quantifying Uncertainty in the BEAVRS Benchmark

Jingang Liang, Shikhar Kumar, Benoit Forget, Kord Smith

Computational Reactor Physics Group, Massachusetts Institute of Technology
jingang@mit.edu, shikhark@mit.edu, bforget@mit.edu, kord@mit.edu

Abstract - *BEAVRS is a highly-detailed PWR model based on two operational cycles of a commercial nuclear power plant. As a benchmark to validate high-fidelity core analysis methods, BEAVRS provides measured reactor data for Hot Zero Power (HZP) physics tests, boron letdown curves, and even three-dimensional in-core flux maps at various burnups during Cycle 1 and Cycle 2. Recent work has been focused on the BEAVRS uncertainty quantification of all the measured data, aiming to make this benchmark a true non-proprietary international benchmark for the validation of high-fidelity tools. This paper details the quantification of flux maps uncertainties through investigation of sources of error in all detector measurements. Detector uncertainties together with errors introduced during data processing such as interpolation and realignment are estimated for all axial measured data and thereby uncertainties of axially integrated radial data are derived. In addition, time series analysis methods are used to calculate time-dependent detector uncertainty data, as an alternative approach to estimating measurement uncertainties.*

I. INTRODUCTION

In recent years, the importance of modeling and simulation has been highlighted extensively in nuclear engineering. Plenty of research efforts aim to develop high-fidelity multi-physics analysis tools for the simulation of current and next-generation nuclear power reactors. Like all analysis tools, verification and validation are essential to guarantee proper functioning of the software and methods employed. Relevant multi-physics benchmark measurements are especially necessary to validate high-fidelity methods being developed today.

BEAVRS [1], proposed by the Computational Reactor Physics Group at the Massachusetts Institute of Technology in 2013, is a highly-detailed PWR benchmark with two cycles of measured operational data used to validate high-fidelity core analysis methods. This PWR depletion benchmark captures the fine details of fuel assemblies, burnable absorbers, in-core fission detectors, core loading and reloading patterns of a commercial nuclear power plant during the first two cycles of operation. It also provides measured reactor data for Hot Zero Power (HZP) physics tests, boron letdown curves, and three-dimensional in-core flux maps from fifty-eight instrumented assemblies, enabling analysts to develop extremely detailed reactor core models that can be used for testing and validation of coupled neutron transport, thermal-hydraulics, and fuel isotopic depletion.

The BEAVRS benchmark specifications and data packages have been publicly released online `http://crpg.mit.edu/`, with continuous updates to reflect more improved knowledge of the core and measured data. The specifications have been used by many groups to assess model parameters and measured data, but the benchmark has been lacking associated uncertainties, thus rendering it difficult for analysts to accurately assess sources of discrepancies in computational results. Recently, a series of uncertainty quantification work has been carried out to address these deficiencies, aiming to make BEAVRS a true non-proprietary international benchmark for the validation of high-fidelity tools.

Since the BEAVRS measurements were performed a long time ago and very little data exists that can be used to evaluate the uncertainties, a variety of methods are used to assess a best estimate of uncertainty. For example, standard deviations of the assembly enrichments are calculated from detailed assembly loadings in two cycles. For the control rod worth and low power physics tests data such as critical boron concentrations and isothermal temperature coefficients, more recent data using similar measurement techniques are used as the basis for quantifying uncertainty. Uncertainty estimation is also made on the hot full power boron let down curves through both statistical analysis and code calculation. A complete and rigorous documentation of the work surrounding BEAVRS uncertainty quantification is planned to be released in the near future.

This paper focuses on uncertainty quantification of the flux maps measured by axial fission detectors at various burnups. The first section investigates sources of error for operational nuclear data and estimates all flux map uncertainties, while the second section uses time-series analysis tools to quantify time-dependent fluctuations in reactor operations as an alternative to estimate the measurement uncertainties.

II. FLUX MAP UNCERTAINTIES

The BEAVRS reactor contains 58 assemblies that can be accessed by in-core detectors through the central guide tubes. Figure 1 shows these positions, where six U-235 fission chambers with varying fissile masses are used to perform the measurements. When measurements are being taken, multiple passes are performed to adequately measure all 58 assemblies. All detectors are passed through one common assembly for signal normalization. The detectors are inserted from the bottom until they reach the top and pulled back to measure the axial fission rate over 61 axial locations.

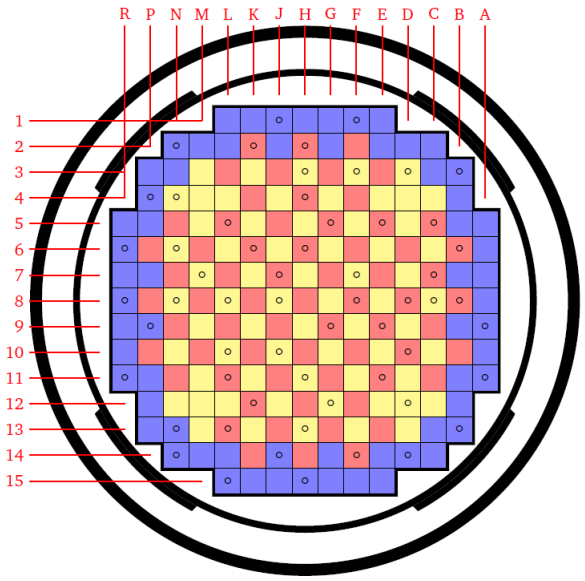

Fig. 1. Instrument tube locations.

1. Extracting Detector Signals and Processing Data

The raw measurement data for one detector in one pass includes 61 axial detector signals, background signal, gain factor of the detector, and core power. The normalized axial flux can be obtained from the detector signals by removing the background, adjusting the gain on the detector and dividing the power, as indicated by Equation 1.

$$\phi_{ijk} = \frac{(D_{ijk} - B_{ij}) \times G_{ij}}{P} \tag{1}$$

where ϕ is the calculated flux, D is the detector signal, B is the background signal, G is the gain factor of the detector, P is the core power, and i, j, k indicate the spatial position of a measurement (i, j for radial assembly position and k for axial location).

Radial assembly flux maps are obtained by integrating over all axial points, as indicated by Equation 2.

$$\phi_{ij} = \sum_{k=1}^{K} \phi_{ijk} \tag{2}$$

However, the measurements are not usable as is and further post-processing is needed to filter the noisy data (such as missing data points and misalignments), which includes:

(1) **Interpolation**: In some of the detector signals, zero points exist where the detector failed to record. These zero points are removed by performing a linear interpolation/extrapolation between/from the nearest two neighbors.

(2) **Re-alignment**: It is observed that not all signals are aligned with each other since the starting position of the recording can differ slightly. However, signals can be realigned according to grid depressions of the signal since grid positions are fixed.

(3) **Spline Fitting**: Detector signals need to be put on an axial coordinate grid corresponding to points that range from the bottom to the top of the active fuel. A second-order spline fit is used to map from measured data axial locations to an axial map with data points exactly at the Top of Active Fuel (TAF) and Bottom of Active Fuel (BAF).

A Python script was developed to do the post-processing of the raw detector data. The final flux maps, including axial distributions and axially integrated radial maps of all 58 assemblies, are generated by this script.

2. Estimating Uncertainty of Axial Detector Data

Generally, both the uncertainty of the measured signals, i.e., detector inaccuracy, and the errors introduced from post-processing should be analyzed and combined to evaluate final uncertainty of the processed data.

The uncertainty of each axial detector data can be expressed using Equations 3 and 4,

$$\begin{aligned}\left(\frac{\delta_\phi}{\phi}\right)_m &= \sqrt{\frac{\left(\frac{\partial\phi}{\partial D}\cdot\delta_d\right)^2 + \left(\frac{\partial\phi}{\partial B}\cdot\delta_b\right)^2 + \left(\frac{\partial\phi}{\partial G}\cdot\delta_g\right)^2 + \left(\frac{\partial\phi}{\partial P}\cdot\delta_p\right)^2}{\phi^2}} \\ &= \sqrt{\frac{{\delta_d}^2 + {\delta_b}^2}{(D-B)^2} + \left(\frac{\delta_g}{G}\right)^2 + \left(\frac{\delta_p}{P}\right)^2}\end{aligned} \tag{3}$$

$$\left(\frac{\delta_\phi}{\phi}\right)_{ijk} = \sqrt{\left(\frac{\delta_\phi}{\phi}\right)_m^2 + \left(\frac{\delta_\phi}{\phi}\right)_{intp}^2 + \left(\frac{\delta_\phi}{\phi}\right)_{align}^2 + \left(\frac{\delta_\phi}{\phi}\right)_{spline}^2} \tag{4}$$

where δ_d, δ_b, δ_g, and δ_p are the uncertainties of the detector signal, background, gain factor, and core power respectively. These sources of uncertainty contribute to the measurement uncertainty $\left(\frac{\delta_\phi}{\phi}\right)_m$, while $\left(\frac{\delta_\phi}{\phi}\right)_{intp}$, $\left(\frac{\delta_\phi}{\phi}\right)_{align}$ and $\left(\frac{\delta_\phi}{\phi}\right)_{spline}$ are the uncertainties introduced from interpolation, realignment and spline fitting.

A. Detector Uncertainties

As shown in Equation 3, the uncertainty of the axial flux has contributions from detector signal, background, gain factor, and the core power measurements.

All types of measured data are gathered and statistical analysis is used to determine the ranges and distributions of the measurements, as shown in Figure 2 for Cycle 1. It is found that:

(1) The background values are very small, mostly provided by readings of 0 or 0.001. Accounting for the smallest division of the detector (0.001), uncertainty of the background can be estimated as half the smallest digit (i.e. $\delta_b = 0.0005$). It should be noted that background is subtracted from detector signal and the detector signal is generally greater than 0.1 (0.41 on average), which implies from Equation 3 that both the effects of B and δ_b are less than 0.1% for most cases.

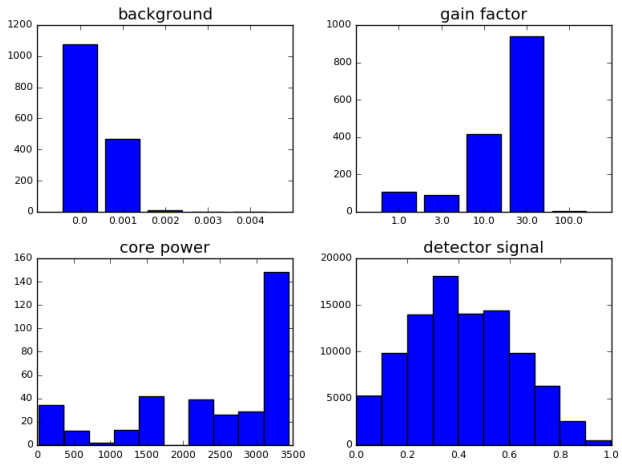

Fig. 2. Ranges and distributions of four types of measured data in Cycle 1.

(2) The gain factors are discrete values which are selected before each pass. As there are only a few well spaced-out values, it is believed that the detector error caused by using different gain factors is negligible compared to other sources, i.e. δ_g is 0.

(3) For almost all of the measurements the core operates at a power on the order of 1000 MWth. As power is very important for normalization and values are reported with decimals, it can be safely assumed that its uncertainty (δ_p) is less than 1.0, which also means that δ_p/P is under 0.1%.

(4) Detector signal is the final component. While the accuracy of the detector is relative to specific measurements, literature indicates that for normal reactor applications the uncertainty is on the order of 1% [2]. Therefore, it can be concluded qualitatively that the detector signal dominates the measurement uncertainty.

Now the question becomes how to evaluate the uncertainty of measured data more accurately. Quantitatively, measurement uncertainty can be evaluated by performing repeated measurements and calculating the variance. Even though the reactor core monitoring is mostly carried out only once for each assembly, there are certain locations that receive multiple measurements for redundancy. For example in Cycle 1 of BEAVRS, there are about 180 cases each that have 2 or even 3 repeated measurements by the same detector in the same assembly. These multiple measurements are performed with the reactor core under almost the same conditions, such as control rod positions, boron concentration, and coolant status. Core power as well as other measured parameters such as background and gain factor of the detector may be slightly different but they will be accounted for in calculating axial flux. So the multiple measurements can be regarded as repeated data and their uncertainty represents the accuracy of the measured data.

Figure 3 is an example of multiple measurements, showing the independent axial signals, mean and relative sample standard deviation (RSTD) of every axial measurement point.

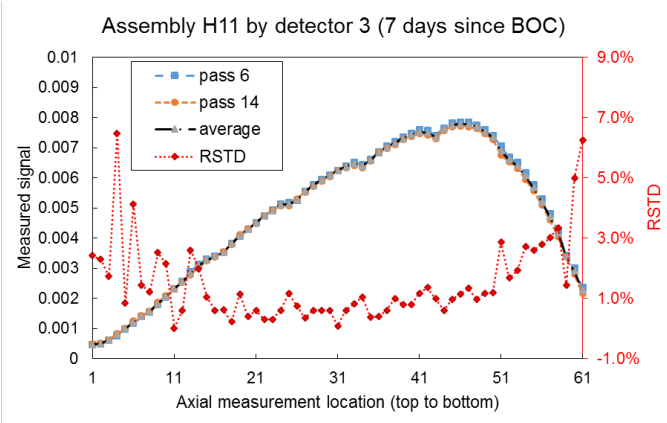

Fig. 3. Multiple measurements example. Assembly H11 was measured twice by Detector 3. The average and relative sample standard deviation (RSTD) is calculated for every axial measurement point.

Since there are only 2 or 3 replicated measurements for each data point, the variance estimate is not likely to be accurate. Thus, gathering the data over all multiple cases and averaging them are necessary to obtain a reliable uncertainty estimate.

Here we assume the measurement uncertainty is related only to the detector signal amplitude. This means that the multiple measurement cases with similar mean value have similar uncertainty, therefore we can group the data points by amplitude and estimate an average uncertainty for each group. Specifically, the relative sample standard deviations are gathered and used to calculate the uncertainties of all groups. To make the estimate more conservative, a 95% confidence value is adopted as the resulting uncertainty. In calculation, all the data are sorted and the value at the 95% position is selected. Note that the data points in one replicated measurement case follow the same Gaussian distribution. For each double repeated measurements case, it can be demonstrated that the relative sample standard deviation follows a distribution given by Equation 5 and the 95% confidence value is actually equal to 2 times the true standard deviation i.e. 2σ.

$$f(s) = \frac{4}{\sqrt{2\pi}\sigma} e^{-\frac{s^2}{\sigma^2}} \tag{5}$$

There are 10725 multiple measurements in Cycle 1 and they are divided into 30 groups by signal amplitude with equal number of data points in each group. The 95% confidence values are calculated for each group, thus a table of signal ranges and measurement uncertainties is obtained, as shown in Figure 4 and Table I.

As can be seen in Figure 4, the axial measurement uncertainty is generally around 2−12% and is dependent on

signal amplitude, i.e. the greater the signal, the smaller the uncertainty. This look-up table will be applied to all detector signals.

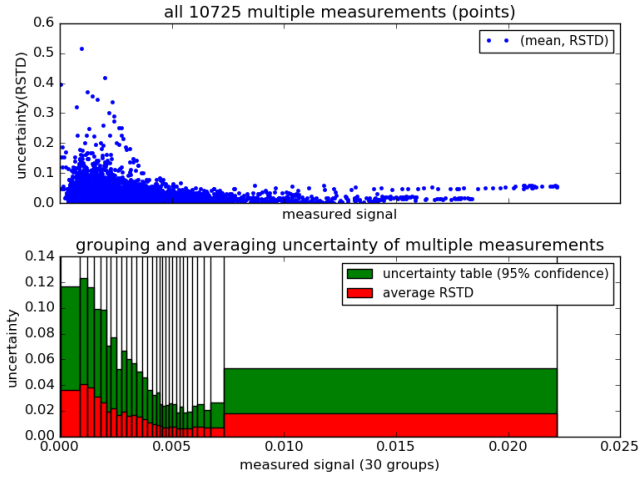

Fig. 4. Axial signal uncertainty from all multiple measurements in Cycle 1. *Top*: A plot of the average and relative sample standard deviation of all multiple measured data points; *Bottom*: A plot that divides the data points into groups and calculates the 95% confidence values for all groups to represent as a measurement uncertainty table.

Figure 5 shows the distribution of uncertainties inside the multiple measurements group, which is roughly consistent with the distribution given by Equation 5.

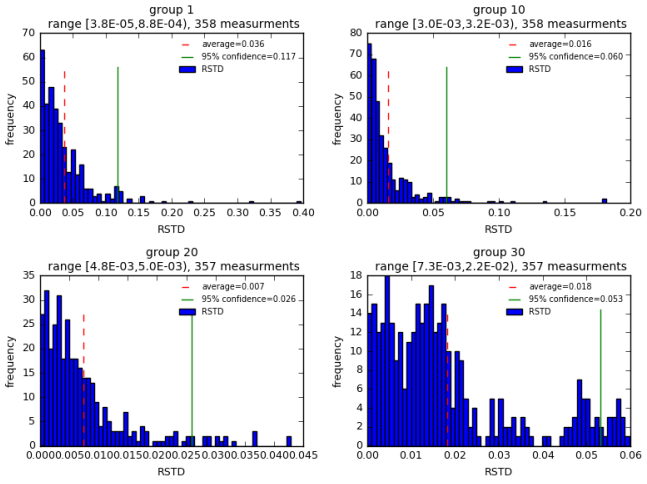

Fig. 5. Distribution of uncertainties inside the multiple measurements groups.

B. Uncertainty from Data Processing

To analyze the uncertainty caused by data post-processing such as interpolation , realignment, and spline fitting, a method of observing the variation before and after the processing is used.

Interpolation

Interpolation is performed when a single data point is unrecorded. To estimate the error of interpolated data, we simply eliminate points that were properly recorded one-by-one and then compare the axial relative error with the recorded data. Figure 6 displays all the interpolation errors and their averages along with axial locations. It is observed that the interpolation error is dependent on location and is greater near endpoints or grid spacers. Here again we use the 95% confidence strategy for each location. The 95% confidence values are collected as a look-up table to estimate the uncertainty of every interpolation performed during processing.

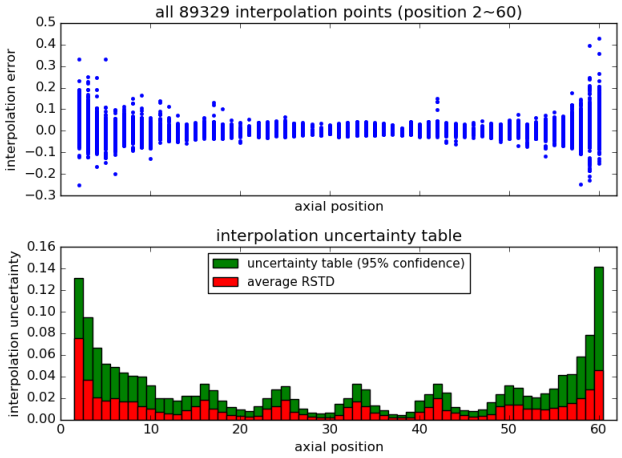

Fig. 6. A representation of axial interpolation uncertainty. *Top*: Interpolation errors along with axial locations. *Bottom*: Interpolation uncertainty table using 95% confidence values for all locations.

Axial Re-alignment

Re-alignment of axial signals is carried out such that axial signals are provided over the active fuel length. The positions of the axial data are moved up or down in re-alignment, with the lost edge points being calculated using extrapolation. Axial measurements are re-aligned by 1 or 2 axial positions, and in some rare situations 3 axial positions. Figure 7 shows an example of the effect of grid re-alignment.

Two sources of error stem from re-alignment. The first part is the error that comes from extrapolation of end points. A similar method of interpolation is used to estimate the error of these extrapolations, i.e. comparing normal measured data with extrapolated data. Figure 8 shows the gathering of extrapolation errors i.e. the relative errors caused by extrapolations in 6 grid positions and the 95% confidence values of these errors. Again, this data will be used as a look-up table to estimate error of axial points which are extrapolated when re-alignment is performed.

group	signal amplitude	uncertainty	group	signal amplitude	uncertainty	group	signal amplitude	uncertainty
1	[3.79E-05, 8.75E-04)	11.7%	11	[3.17E-03, 3.40E-03)	5.7%	21	[5.00E-03, 5.18E-03)	2.5%
2	[8.75E-04, 1.21E-03)	12.4%	12	[3.40E-03, 3.65E-03)	5.0%	22	[5.18E-03, 5.35E-03)	1.8%
3	[1.21E-03, 1.53E-03)	11.6%	13	[3.65E-03, 3.88E-03)	4.6%	23	[5.35E-03, 5.50E-03)	2.3%
4	[1.53E-03, 1.83E-03)	9.9%	14	[3.88E-03, 4.10E-03)	3.6%	24	[5.50E-03, 5.68E-03)	1.8%
5	[1.83E-03, 2.07E-03)	9.9%	15	[4.10E-03, 4.29E-03)	3.2%	25	[5.68E-03, 5.88E-03)	1.9%
6	[2.07E-03, 2.26E-03)	7.1%	16	[4.29E-03, 4.44E-03)	3.4%	26	[5.88E-03, 6.13E-03)	2.4%
7	[2.26E-03, 2.51E-03)	7.7%	17	[4.44E-03, 4.57E-03)	2.5%	27	[6.13E-03, 6.41E-03)	2.5%
8	[2.51E-03, 2.73E-03)	5.2%	18	[4.57E-03, 4.70E-03)	2.4%	28	[6.41E-03, 6.73E-03)	2.1%
9	[2.73E-03, 2.96E-03)	6.7%	19	[4.70E-03, 4.85E-03)	2.5%	29	[6.73E-03, 7.31E-03)	2.6%
10	[2.96E-03, 3.17E-03)	6.0%	20	[4.85E-03, 5.00E-03)	2.6%	30	[7.31E-03, 2.22E-02)	5.3%

TABLE I. Measurement uncertainty table in Cycle 1.

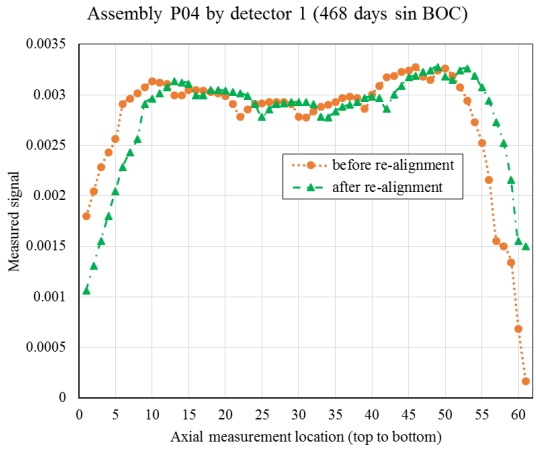

Fig. 7. Example of re-alignment error.

Secondly, even after all the signals are re-aligned, the measured locations themselves can be erroneous due to the fluctuations of starting positions or the detector moving speeds. During the re-alignment, it is found that more than half of the assemblies are shifted by 1 or more axial measured grids. To simplify the problem, here we assume that, at 95% confidence, the uncertainty of the measurement position is within one measured grid length, i.e., every measurement point can be wrongly recorded as much as its upper or lower point. Therefore, the position-related uncertainty of each signal can be calculated as the larger error between the current point and its two neighboring points. It should be noted the positional error is sensitive to the location or the variation of of the signal. In a flat region like the middle core, the signal may change about 1% within one grid while around the endpoints this number can be as high as 30%. The re-alignment uncertainty is determined as the combination of extrapolation error and position error.

Spline Fitting

Spline fitting is used to put the detector signals on an axial coordinate grid corresponding to points that range from the bottom to the top of the active fuel. The error introduced in spline fitting is found negligible because the second order

Fig. 8. A representation of axial extrapolation uncertainty. *Top*: Distribution of extrapolation errors for 6 axial locations. *Bottom*: Extrapolation uncertainty table using 95% confidence values for all locations.

spline fit is quite accurate and the errors are less than 10^{-10}.

$$\left(\frac{\delta_\phi}{\phi}\right)_{spline} \approx 0 \tag{6}$$

C. Combining Uncertainties

Finally, the uncertainties of all axial signals can be quantified by calculating all independent uncertainties using the look-up tables and combining them together using the uncertainty Equation 4. Specifically, the following steps will be performed for every axial signal.

(1) The measurement uncertainty $\left(\frac{\delta_\phi}{\phi}\right)_m$ is determined according to the amplitude of calculated axial data.

(2) If this data point is interpolated, an interpolation error $\left(\frac{\delta_\phi}{\phi}\right)_{intp}$ is determined according to its location on the lookup table.

(3) If this data point is realigned, an extrapolation error $\left(\frac{\delta_\phi}{\phi}\right)_{align}$ is determined according to its location. Furthermore, the measured position uncertainty is calculated as

the larger error between the current signal and its two neighboring points.

(4) The square root of sum of squares of all uncertainties is calculated as the resulting uncertainty $\left(\frac{\delta_\phi}{\phi}\right)_{ijk}$ for each data point.

Figures 9 and 10 show combined axial signal uncertainty for two assemblies in Cycle 1 and Cycle 2 respectively. As can be seen from the two figures, the axial measurement uncertainty has a large range based on location, just like the signal itself. But for most of the measured data, the main contribution to the uncertainty is from the detector inaccuracy and position error. This value is generally around 3 to 5%. For the endpoints, the relative uncertainties increase noticeably since the signals are small and sensitive to location.

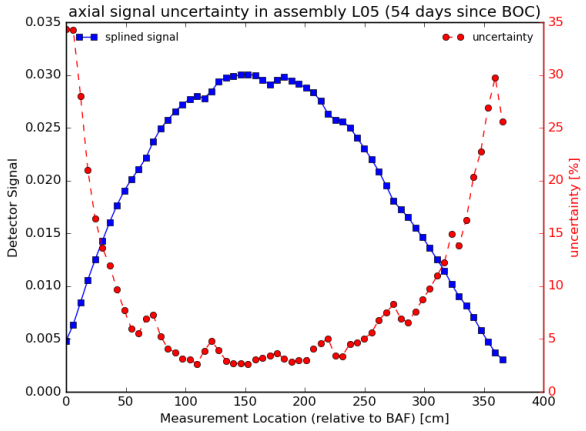

Fig. 9. Combined uncertainty of axial detector measurement - Assembly L05 on Day 54 in Cycle 1.

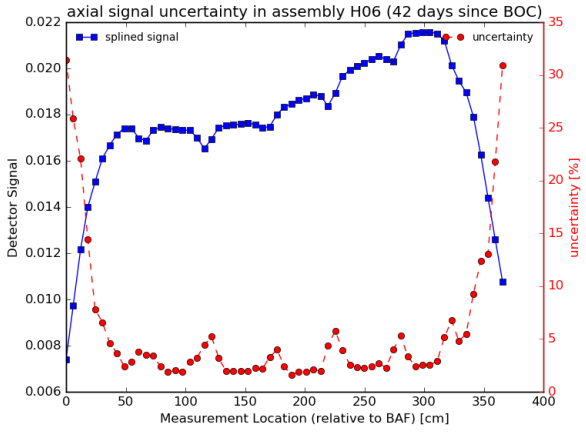

Fig. 10. Combined uncertainty of axial detector measurement - Assembly H06 on Day 42 in Cycle 2.

3. Uncertainty of Axially Integrated Radial Data

Uncertainty of axially integrated radial assembly data can be evaluated by accounting for the errors of all axial points in one assembly, as indicated by Equation 7,

$$\left(\frac{\delta_\phi}{\phi}\right)_{ij} = \frac{\sqrt{\sum_{k=1}^{K}\left(\delta_\phi\right)_{ijk}^{2}}}{\phi_{ij}} \tag{7}$$

where i, j represent the radial assembly position and k the axial location.

For example, in Assembly L05 shown in Figure 9, an integrated uncertainty of 0.83% is obtained by substituting the axial uncertainties into the equation.

The uncertainties of all assembly data at all burnups are calculated this way. Figure 11 gives the full core radial detector measurements together with the calculated uncertainties under HZP conditions in Cycle 1. Furthermore, by gathering all assembly uncertainties in the whole cycle, it is found the average uncertainty of radial measurements is around 1.0% for both Cycle 1 and Cycle 2 and the 95% confidence value is 1.4%.

The multiple measurements can also be used to quantify uncertainty of radial data in a different way. Similar to the treatment with the axial multiple signals, all multiple measurement cases of radial data are collected and statistics computed to estimate uncertainty of radial data, as shown in Figure 12. There are 179 cases of multiple measurements in Cycle 1. The 95% confidence value is 1.8%. Note again that the distribution of RSTD of the multiple measurement is consistent with the theoretical analysis, i.e. using Equation 5.

It should be noted that the two ways to estimate radial uncertainty are somewhat independent and can be compared against each other. Figures 13 and 14 compare the assembly uncertainty distributions obtained from both approaches for Cycle 1 and Cycle 2 respectively. It can be seen that the two ways give similar 95% confidence uncertainties for both cycles, which reaffirms the provided value as a good estimate. Note that the calculated uncertainty distributions in the lower figures are much different from the upper distributions of multiple measurement RSTD's. This is not surprising since the calculated uncertainty is the expectation of real uncertainties. All the assemblies have similar flux and are measured by the same set of detectors so the uncertainties roughly follow a Gaussian distribution.

III. MEASURING TIME-DEPENDENT UNCERTAINTY

The uncertainty quantification work that has been performed so far has dealt with analyzing the sources of uncertainty at individual burnups, where each burnup step is regarded as independent of neighboring burnup steps. However, this section aims to characterize how reaction rates vary

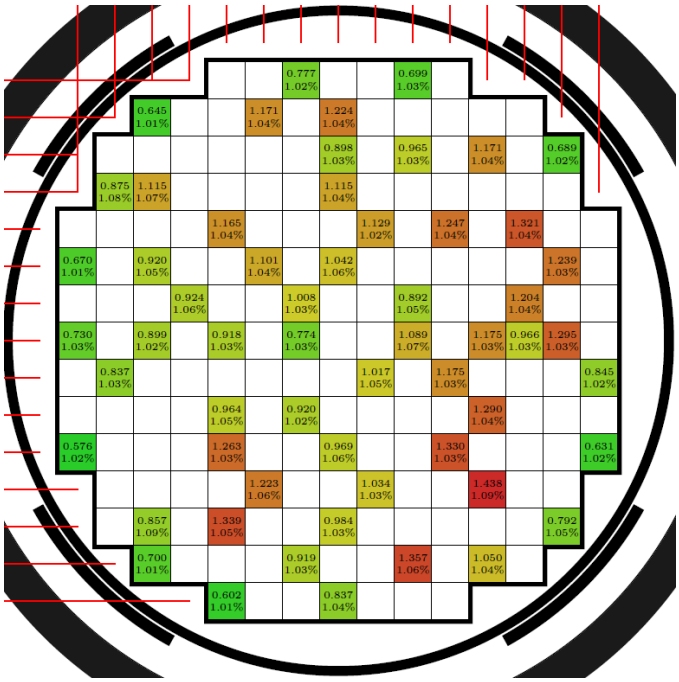

Fig. 11. Radial assembly measurements with uncertainties calculated from axial uncertainties at HZP in Cycle 1. The top number is normalized assembly signal while the bottom number is its uncertainty.

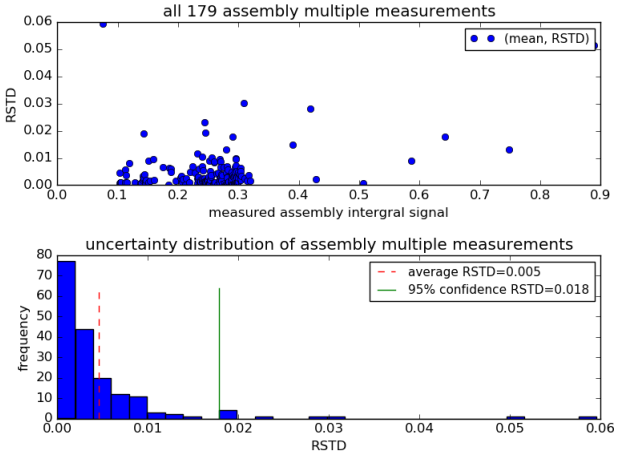

Fig. 12. Distribution of radial data uncertainty calculated from axial uncertainties in Cycle 1.

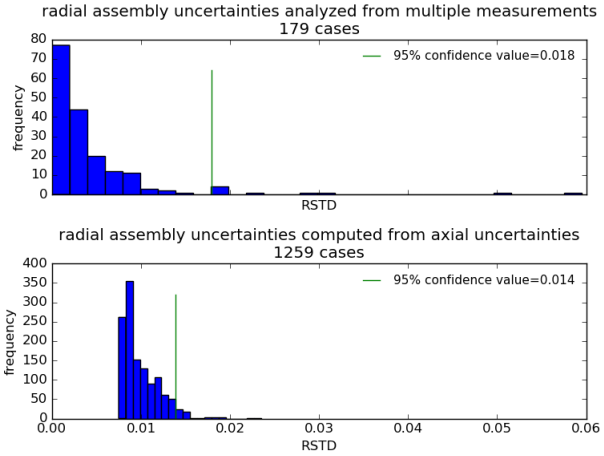

Fig. 13. Comparison of assembly uncertainty distributions obtained from two approaches in Cycle 1.

over short time intervals using predictive models in order to determine whether calculated reaction rates follow any observable trend. By fitting BEAVRS data to such trends, any deviation from these trends can be regarded as an alternative method for uncertainty quantification. For this section, time-dependent trends are best modeled when core conditions are approximately at full power and not interrupted by temporary shutdowns and sudden fluctuations, so the burnup set is restricted to those points above 90% power. Figures 15 and 16 illustrate the full set of burnup points in Cycle 1 and 2 respectively, where the green points denote full power points.

Previous BEAVRS uncertainty quantification work looked at using linear models to fit BEAVRS data [3]. While this was an accurate model for first-order fitting, using a linear regression model was not wholly accurate due to the volatile power history for Cycle 1 that calls in question the steady-state requirements for such fitting to be appropriate. Moreover, a linear fit cannot be conducted without knowing the BEAVRS reaction rates a priori, and neglects taking into account any of the actual operating conditions within the reactor. Instead,

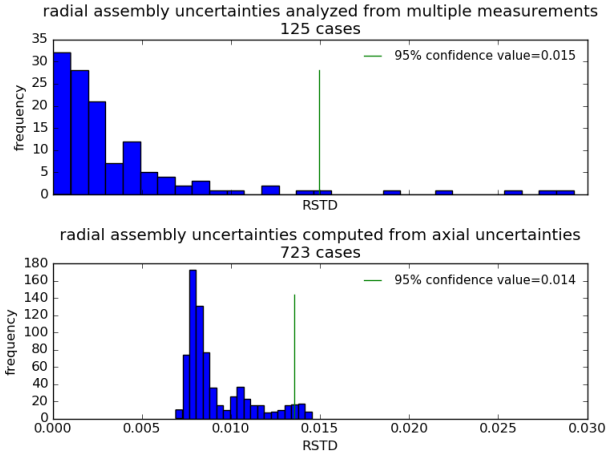

Fig. 14. Comparison of assembly uncertainty distributions obtained from two approaches in Cycle 2.

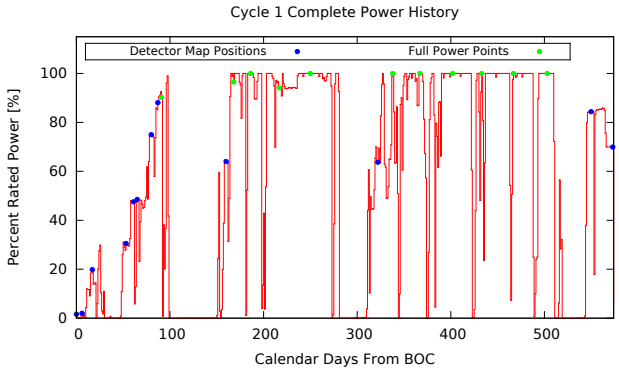

Fig. 15. Cycle 1 burnup points. Full power points are indicated by green points (above 90% power). The list of full power points (in MWd/kg) are 1.02, 1.51, 2.16, 3.30, 4.61, 6.49, 7.51, 8.70, 9.80, 11.08, 12.34.

this paper focuses on using more predictive models that can be used to capture higher-order effects observed within the reactor. Before such discussions, however, the role of tilt-correction on BEAVRS reaction rates data must be explained.

1. Correcting for Tilt at Hot Zero Power

BEAVRS data contains a significant NW-SE tilt at HZP despite a symmetric core loading pattern. This asymmetry cannot be explained merely by errors in detector measurements. This creates an issue since simulations for core calculations typically produce symmetric results for symmetric core loading patterns. Thus, comparing BEAVRS data to data from deterministic codes creates a systemic error due to this tilt. The leading hypothesis to explain this tilt is that an uneven distribution of water gaps was introduced during core loading. It is possible to induce such a tilt in simulation tools and compare this data to post-processed BEAVRS data, however the

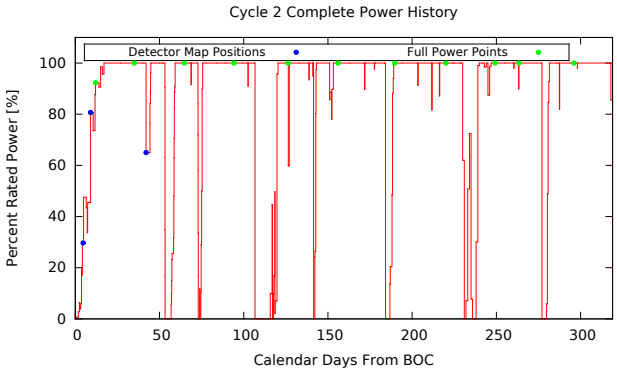

Fig. 16. Cycle 2 burnup points. Full power points are indicated by green points (above 90% power). The list of full power points (in MWd/kg) are 0.23, 1.14, 2.11, 3.20, 4.04, 5.23, 6.52, 7.71, 8.73, 9.36, 10.43.

exact source of this error is not exactly known. Instead, the tilt in BEAVRS data is corrected for in order to make the reaction rates eighth-core symmetric, and this correction needs to be accounted for as as an additional source of error. For every burnup, the best x-y plane that fits the 58 measurements is found and adjusted for. Moreover, once this tilt is removed, symmetric positions are extrapolated from known readings, as the radial reaction rate map is now symmetric. The magnitude of the tilt decreases over burnup for both Cycle 1 and Cycle 2 [4]. The following section utilizes tilt-corrected BEAVRS data as a basis for comparison to data from simulation tools.

2. Fitting Data from Simulation Codes to BEAVRS Data

Time-dependent BEAVRS uncertainty quantification work initially used linear models to fit data for reaction rates over burnup, and then transitioned to using reaction rates from CASMO-5 lattice codes [5] and Simulate-3 nodal diffusion simulator [6] as an additional basis for comparing to BEAVRS data. It was observed that using CASMO/Simulate results predicted the proper shape of burnup trends but induced a persisting bias due to the methodologies and assumptions embedded into the simulation models [3]. The discrepancy was attributed as model bias, and this section serves to quantify time-dependent uncertainty by correcting for this model bias over short burnup intervals.

For the purposes of this analysis, only a subset of burnups are going to be examined, as the highly volatile power history makes it difficult to model reaction rates effectively over a long burnup. Looking at a smaller burnup set does indicate that there is higher precision in modeling phenomena than a simple linear model.

Figure 17 plots reaction rates for CASMO/Simulate and BEAVRS data for Assembly D10 at burnups 1.02, 1.51, and 2.16 MWd/kgHM. Looking at this region, it is clear that the two plots behave similarly but are offset by some amount. Defining this offset as model bias, the goal is to overlay the

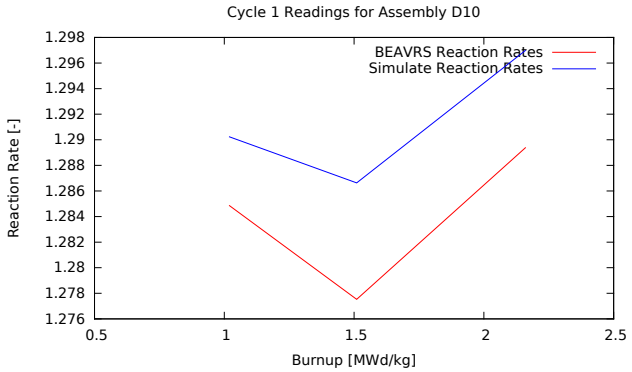

Fig. 17. Reaction rates for CASMO/Simulate and BEAVRS data for Assembly D10 at 1.02, 1.51, and 2.16 MWd/kg.

BEAVRS data onto the CASMO/Simulate data, and then measure how much noise there is between this new data set and CASMO/Simulate. This noise can be quantified as a measure of time-dependent uncertainty. This is done for all assemblies over a subset of burnups for both cycles. The results for burnup range 1.02, 1.51, and 2.16 MWd/kgHM in Cycle 1 are summarized in Figure 18. RMS for model bias for the entire core for this burnup range is 1.8%, while the RMS for time-dependent uncertainty is 0.9%

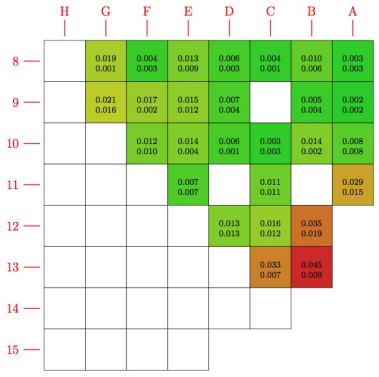

Fig. 18. Time-dependent uncertainty (top) and model bias (bottom) values using CASMO/Simulate model for each assembly over cycle 1 burnups of 1.02, 1.51, and 2.16 MWd/kg. Assembly-weighted Model Bias: 0.018, Assembly-weighted Time-Dependent Uncertainty: 0.009.

Assuming that burnup sets with non-overlapping points are independent of each other, Simulate data is fit to the entire burnup range, dividing the entire range into three subsets. For Cycle 1, the entire burnup set is subdivided into the three burnup ranges of [1.02, 1.51, 2.16], [3.30, 4.61, 6.49, 7.51], and [8.70, 9.80, 11.08, 12.34] and error between Simulate and BEAVRS is aggregated for these three subdivisions on the same histogram. Similarly for Cycle 2, the entire burnup range is subdivided into the subsets [0.23, 1.14, 2.11], [3.20, 4.04, 5.23, 6.52], and [7.61, 8.73, 9.36, 10.43]. Subdivision of the entire burnup range is carried out in this manner since it is believed that measurements errors would dominate over short intervals but other physical deviations could come into play over longer intervals that could mask the measurement error. Figure 19 plots these errors between BEAVRS data and SIMULATE data for Cycle 1, where the data is weighted by the number of symmetric assembly positions.

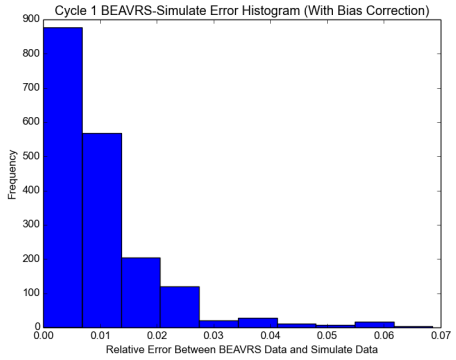

Fig. 19. Histogram of relative error distributions over entire burnup rate of Simulate Data vs. BEAVRS data with bias correction for Cycle 1. RMS = 1.4%, 95% level = 2.7%.

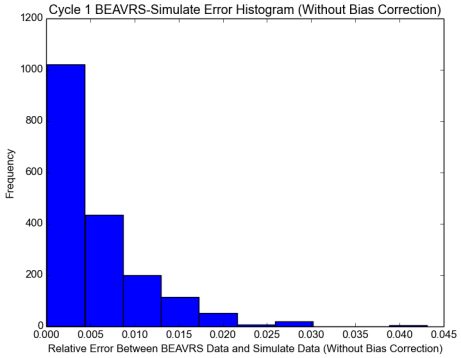

Fig. 20. Histogram of relative error distributions over entire burnup rate of Simulate Data vs. BEAVRS data without bias correction for Cycle 1. RMS = 0.8%, 95% level = 1.6%.

From this histogram, it is clear that errors are skewed towards the lower end, with a few large outliers on the higher end. The RMS value for Cycle 1 is 1.4%, but taking a more conservative error estimate of 95% confidence yields a much higher error of 2.7% for Cycle 1. The main issue with using these results is that the error between BEAVRS and Simulate includes model bias. Figure 20 corrects for this bias over short burnup intervals and plots the error between Simulate and BEAVRS data with bias correction on a single histogram. The 95% confidence value of time-dependent uncertainty now is 1.6% for Cycle 1, and following a similar procedure for Cycle 2 yields a time-dependent uncertainty of 0.9%. The authors interpret these results as suggesting that if model bias could be completely corrected for, then the resulting time-dependent

Burnup Subdivision			Time-Dependent Uncertainty
Cycle 1			
(1.02 1.51 2.16)	(3.3 4.61 6.49 7.51)	(8.7 9.8 11.08 12.34)	1.6%
(1.02 1.51 2.16 3.3)	(4.61 6.49 7.51)	(8.7 9.8 11.08 12.34)	1.7%
(1.02 1.51 2.16 3.3)	(4.61 6.49 7.51 8.7)	(9.8 11.08 12.34)	1.6%
Cycle 2			
(0.23 1.14 2.11)	(3.2 4.04 5.23 6.52)	(7.71 8.73 9.36 10.43)	0.9%
(0.23 1.14 2.11 3.2)	(4.04 5.23 6.52)	(7.71 8.73 9.36 10.43)	1.0%
(0.23 1.14 2.11 3.2)	(4.04 5.23 6.52 7.71)	(8.73 9.36 10.43)	0.9%

TABLE II. Sensitivity analysis of time-dependent uncertainty and model bias based on burnup subdivison of each cycle.

uncertainty due to fitting data from reactor analysis software to operational data is on the same order as axially integrated measurement uncertainty. The uncertainty that arises from measurement carries over throughout the core burnup and can be used to explain the random fluctuations that occur when trying to fit time-dependent trends.

To show that these results are not overly dependent on how subdivisions are made, the same analysis is performed by perturbing the subdivision endpoints. Table II summarizes the results for 95% confidence time-dependent uncertainty from data fitting to CASMO/Simulate, and it is clear that these results are independent of burnup choice, as long as the entire burnup range for the cycle is included. Thus, the 95% confidence value of 1.6% to 1.7% for Cycle 1 and 0.9% to 1.0% for Cycle 2.

IV. CONCLUSIONS

The BEAVRS benchmark has been instrumental in showing the efficacy of high fidelity modeling tools to model realistic PWR models. Recent work has been focused on quantifying the uncertainty in areas of data measurement, data processing, and time-series uncertainty. The flux map uncertainties are obtained through a close investigation of sources of error for all detector measurements. The results indicate that axial measurement uncertainty is dependent on signal amplitude and measured location, most of which is around 3% to 5% at the 95% confidence level. Radial assembly signal uncertainties are also analyzed using three independent approaches: sum of axial uncertainties, statistics on multiple axially integrated data, and time-dependent uncertainties. Results are summarized in Table III and demonstrate consistency between the three approaches.

Future work involves looking at how model bias affects results for each assembly. This includes more concrete values for uncertainty from tilt-correction, as well as obtaining data from WIMS/Panther codes to use as an additional basis for comparison between BEAVRS data when calculating time-dependent uncertainty. The ultimate objective in using WIMS/Panther results instead of CASMO/Simulate is to show that time-dependent uncertainty remains consistent regardless of the simulation tools being used to predict reaction rates over burnup. Such results bring more credence to using nuclear codes to predict higher order effects observed within actual reactor operations. Any further discrepancies that arise after correcting for model bias should solely be due to the uncertainty in the underlying BEAVRS data, namely from measurement and post-processing data.

	Method of Uncertainty Quantification		
	Multiple Measurements	Theoretical Analysis of Axial Uncertainties	Fitting Simulate Burnup Trends to BEAVRS data
Cycle 1	1.8%	1.4%	1.6%
Cycle 2	1.5%	1.4%	0.9%

TABLE III. Summary of results from uncertainty quantification using three independent methods.

V. ACKNOWLEDGMENTS

Partial funding for the development of this benchmark comes from a Nuclear Energy University Program Grant from the Department of Energy. The authors would also like to thank Studsvik Scandpower for providing access to CASMO/Simulate data and Dr. Koroush Shirvan for his continued help with this project.

REFERENCES

1. N. E. HORELIK, B. R. HERMAN, B. FORGET, and K. SMITH, "Benchmark for Evaluation and Validation of Reactor Simulations," in "International Conference on Mathematics and Computational Methods Applied to Nuclear Science & Engineering (M&C 2013)," (2013).
2. M. MITELMAN, "In-core monitoring detectors," Tech. rep. (2001).

3. S. KUMAR, J. LIANG, B. FORGET, and K. SMITH, "Quantifying Transient Uncertainty in the BEAVRS Benchmark Using Time Series Analysis Methods," *Transactions of the American Nuclear Society*, **115**, 1093 (2016).
4. J. LIANG, K. SHIRVAN, M. RATHBUN, M. ELLIS, H. LEE, B. FORGET, and K. SMITH, "Integral Full Core Multi-Physics PWR Benchmark with Measured Data BEAVRS UQ NEUP 14-6742: Year 1 Report," Tech. rep., Massachusetts Institute of Technology (2015).
5. J. RHODES, K. SMITH, and D. LEE, "CASMO-5 development and applications," in "Proc. ANS Topical Meeting on Reactor Physics (PHYSOR-2006)," (2006), pp. 10–14.
6. J. CRONIN, K. SMITH, D. VER PLANCK, J. UMBARGER, and M. EDENIUS, "SIMULATE-3 Methodology, Advanced Three-Dimensional Two-Group Reactor Analysis Code," *Studsvik/SOA-95/18, Studsvik of America, Inc* (1995).